

Benchmarking the Inert Doublet Model for e^+e^- colliders

Jan Kalinowski,^{a,b} Wojciech Kotlarski,^c Tania Robens,^d Dorota Sokołowska^a
and Aleksander Filip Żarnecki^a

^a *Faculty of Physics, University of Warsaw, ul. Pasteura 5, 02-093 Warsaw, Poland*

^b *Deutsches Elektronen-Synchrotron, Notkestrasse 85, 22607 Hamburg, Germany*

^c *Institut für Kern- und Teilchenphysik, TU Dresden, 01069 Dresden, Germany*

^d *MTA-DE Particle Physics Research Group, University of Debrecen, 4010 Debrecen, Hungary*

Abstract

In this short note we present benchmarks for the Inert Doublet Model, a Two Higgs Doublet Model with a dark matter candidate. They are consistent with current constraints on direct detection, including the most recent bounds from the XENON1T experiment and relic density of dark matter, as well as with known collider and low-energy limits. We focus on parameter choices that promise detectable signals at lepton colliders via pair-production of H^+H^- and HA . For these we choose a large variety of benchmark points with different kinematic features, leading to distinctly different final states in order to cover the large variety of collider signatures that can result from the model.

1 Introduction

The results from the ATLAS and CMS collaborations from Run I and ongoing Run II are in good agreement with the predictions of the Standard Model (SM) [1, 2]. Although the discovered Higgs particle appears to be consistent with the expectations for a SM Higgs boson, both the experimental uncertainties and theoretical speculations still leave room for new physics. In particular the scalar sector can provide intriguing scenarios in this respect which should be further scrutinized.

Although experimental collider data is in good agreement with predictions of the Standard Model alone, a number of non-collider observations can only be described in models containing additional (new physics) constituents. A prime example for this is dark matter (DM). Within the standard model of cosmology, the Planck mission data [3] implies that nearly 85% of the total matter content in the universe is dark. However, so far only the gravitational interactions of these hypothetical particles have been detected, and a fundamental nature of DM remains largely unknown. Since the Standard Model of elementary particles does not contain a viable DM candidate, any evidence of DM in the direct detection or indirect detection experiments or production at colliders would be a signal of new physics, the discovery of which is arguably one of the most important goals in the field.

An intriguing extension of the SM scalar sector is the Inert Doublet Model (IDM) which features a dark matter candidate [4–6]. In this two Higgs doublet model a discrete Z_2 symmetry (called D -symmetry) is imposed, with the following transformation properties:

$$\phi_S \rightarrow \phi_S, \phi_D \rightarrow -\phi_D, \text{ SM} \rightarrow \text{SM}, \quad (1)$$

where the ϕ_S doublet plays the same role as the corresponding doublet in the SM, providing the SM-like Higgs particle. This doublet is even under the D -symmetry, while the second doublet, the inert (or dark) ϕ_D , is D -odd and contains four scalars, two charged and two neutral ones, labelled H^\pm and H, A , respectively. The above symmetry renders the additional $SU(2)_L$ doublet ϕ_D inert, *i.e.* prevents its couplings to the SM matter sector, thereby providing a dark matter candidate. In the rest of this work, we consider cases where H serves as the dark matter candidate of the model.

The IDM was first discussed in [4] and later in [5, 6]. The model was further studied in [7–11], followed with further analyses of the IDM at colliders [11–32].

We here present a set of the IDM benchmarks proposed for detailed studies at the future e^+e^- colliders ILC and CLIC. They have been selected from updates of the scan presented in [23, 31] and represent distinct features for two prominent production processes at linear colliders, $e^+e^- \rightarrow H^+H^-$ and $e^+e^- \rightarrow AH$. Our benchmarks are designed to cover all interesting parameter space, featuring different mass splittings between H and other dark particles, leading to distinct collider signatures.

The outline of this paper is as follows. We start with a short description of the IDM in section 2, followed with a discussion of current experimental limits in section 3. In section 4 we define benchmark points that pass all constraints and discuss their applications to further studies at linear colliders.

2 The IDM

The scalar sector of the IDM consists of two $SU(2)_L$ doublets of complex scalar fields, ϕ_S and ϕ_D , with the D -symmetric potential:

$$V = -\frac{1}{2} \left[m_{11}^2 (\phi_S^\dagger \phi_S) + m_{22}^2 (\phi_D^\dagger \phi_D) \right] + \frac{\lambda_1}{2} (\phi_S^\dagger \phi_S)^2 + \frac{\lambda_2}{2} (\phi_D^\dagger \phi_D)^2 \\ + \lambda_3 (\phi_S^\dagger \phi_S) (\phi_D^\dagger \phi_D) + \lambda_4 (\phi_S^\dagger \phi_D) (\phi_D^\dagger \phi_S) + \frac{\lambda_5}{2} \left[(\phi_S^\dagger \phi_D)^2 + (\phi_D^\dagger \phi_S)^2 \right]. \quad (2)$$

Exact D -symmetry implies that only ϕ_S can acquire a nonzero vacuum expectation value (v). As a result the scalar fields in ϕ_D do not mix with the SM-like field from ϕ_S , and the lightest particle of the dark sector is stable. The dark sector contains four new particles: H , A and H^\pm . We here choose H to denote the dark matter candidate¹.

After electroweak symmetry breaking, the model contains seven free parameters. Agreement with the Higgs boson discovery and electroweak precision observables fixes the SM-like Higgs mass M_h and v , and we are left with five free parameters, which we take as

$$M_H, M_A, M_{H^\pm}, \lambda_2, \lambda_{345}, \quad (3)$$

¹ A priori, any of the new scalars can function as a dark matter candidate. However, we neglect the choice of a charged dark matter candidate, as these are strongly constrained [33]. Choosing A instead of H changes the meaning of λ_5 , with rephasing of $\lambda_5 \rightarrow -\lambda_5$, but not the overall phenomenology of the model, cf. [23].

where the λ 's refer to couplings within the dark sector and to the SM-like Higgs respectively. In the following, we will use the abbreviation $\lambda_{345} = \lambda_3 + \lambda_4 + \lambda_5$.

3 Experimental and theoretical constraints

In this work, we make use of the tool chain used in [23], and explicitly follow the scan procedure described therein; however, we update several constraints as discussed below. Explicit benchmark points (BP) for the IDM, taking all constraints viable at that time into account, have been presented in [23, 34], which focus on processes at the LHC; some of these were already investigated in a linear collider context in [24]. Ref. [31] shows how the available parameter space for certain scenarios is further limited by more recent constraints.

As the experimental constraints have evolved significantly since that time, we decided to define the new set of benchmark points, fulfilling the updated constraints and focused on the detailed analysis of e^+e^- collider sensitivity. Unless stated otherwise, all considered BP fulfil the latest experimental limits; following [23] (see also the discussion in [35]), we do not require the IDM to provide 100% of the dark matter relic density. Below we briefly summarize the imposed constraints, emphasizing on updates with respect to [23], and describe the set-up to find good BP and discuss the obtained limits.

3.1 Theoretical and experimental constraints

Positivity constraints: we require that the potential is bounded from below, therefore no field configuration leads to $V \rightarrow -\infty$, resulting in tree-level relations [36]

$$\lambda_1 > 0, \lambda_2 > 0, \lambda_3 + \sqrt{\lambda_1 \lambda_2} > 0, \lambda_{345} + \sqrt{\lambda_1 \lambda_2} > 0. \quad (4)$$

These relations hold on tree level and in this work we do not consider higher order contributions, which in principle could lead to change in stability of the electroweak vacuum [10, 37].

Perturbative unitarity: we require the scalar $2 \rightarrow 2$ scattering matrix to be unitary, i.e. all eigenvalues of scattering matrices for scalars with specific hypercharge and isospin should satisfy $|L_i| \leq 16\pi$ [38, 39]. Furthermore, we require all quartic scalar couplings to be perturbative, i.e. to take absolute values $\leq 4\pi$.

Global minimum: in the IDM two neutral minima can coexist even at tree level. Unless the following relation is satisfied

$$\frac{m_{11}^2}{\sqrt{\lambda_1}} \geq \frac{m_{22}^2}{\sqrt{\lambda_2}}, \quad (5)$$

the inert minimum is only a local one, with the global vacuum corresponding to the case of massless fermions [40]. We impose the above relation in our scan.

Higgs mass and signal strengths: the mass of the SM-like Higgs boson h is set to

$$M_h = 125.1 \text{ GeV},$$

in agreement with limits from ATLAS and CMS experiments [41, 42], while the total width of the SM-like Higgs boson obeys an upper limit of [43]

$$\Gamma_{\text{tot}} \leq 13 \text{ MeV}. \quad (6)$$

In the IDM, the total width of the SM-like state can obtain modifications from the following two contributions. For dark matter masses $M_H \leq M_h/2$, invisible decays of the 125 GeV resonance can lead to large additional contributions. Therefore, in these scenarios the above bound poses one of the most dominant constraints, especially affecting λ_{345} [23, 31]. Furthermore, the partial decay width of h to diphoton final states can be altered significantly [11, 19], as the new physics corrections are formally of the same order as the SM process. This leads to a clear distinction between allowed and forbidden regions in the $(\lambda_{345}, M_{H^\pm})$ plane [23, 31]. The Run I combined ATLAS and CMS limit for $h \rightarrow \gamma\gamma$ signal strength is given by $\mu_{\gamma\gamma} = 1.14^{+0.38}_{-0.36}$ [44]. In our analysis we use both the upper limit (6) and require agreement within 2σ for the prediction of $h \rightarrow \gamma\gamma$. We furthermore check agreement with all other branching ratios of the 125 Higgs on the 2σ level using the publicly available tool `HiggsSignals-2.2.1beta` [45], and require $\Delta\chi^2 \leq 11.31$, corresponding to a 95% confidence level.

Gauge bosons width: introduction of light new particles could in principle significantly change the total width of electroweak gauge bosons (cf. e.g. [46]). To ensure that $W^\pm \rightarrow HH^\pm$ and $Z \rightarrow HA, H^+H^-$ decay channels are kinematically forbidden we set:

$$M_{A,H} + M_{H^\pm} \geq M_W, M_A + M_H \geq M_Z, 2M_{H^\pm} \geq M_Z. \quad (7)$$

Electroweak precision tests (EWPT): we call for a 2σ (i.e. 95% C.L.) agreement with electroweak precision observables, parametrized through the electroweak oblique parameters S, T, U [47–50]. In our work, calculations were done through the routine implemented in the Two Higgs Doublet Model Calculator (2HDMC) tool [51], which checks whenever model predictions fall within the observed parameter range [52].

Charged scalar mass and lifetime: we take a conservative lower estimate on the mass of M_{H^\pm} following analysis in [53] to be

$$M_{H^\pm} \geq 70 \text{ GeV}. \quad (8)$$

We also set an upper limit on the charged scalar lifetime of $\tau \leq 10^{-7} \text{ s}$, in order to evade bounds from quasi-stable charged particle searches. This translates to a lower bound on the total decay width of the charged scalar H^\pm of $\Gamma_{\text{tot}} \geq 6.58 \times 10^{-18} \text{ GeV}$.

Collider searches for new physics: we require agreement with the null-searches from the LEP, Tevatron, and LHC experiments. We use the publicly available tool `HiggsBounds-5.2.0beta` [54–57]. In addition the reinterpreted LEP II searches for supersymmetric particles analysis exclude the region of masses in the IDM where simultaneously [12]

$$M_A \leq 100 \text{ GeV}, M_H \leq 80 \text{ GeV}, \Delta M(A, H) \geq 8 \text{ GeV}, \quad (9)$$

as it would lead to a visible di-jet or di-lepton signal. After taking into account all the above limits we are outside of the region excluded due to the reinterpretation of the supersymmetry analysis from LHC Run I [21].

Dark matter phenomenology: we apply dark matter relic density limits obtained by the Planck experiment [3]:

$$\Omega_c h^2 = 0.1197 \pm 0.0022. \quad (10)$$

For a DM candidate that provides 100% of observed DM in the Universe we require the above bound to be fulfilled within the 2σ limit. However, we also allow for the case where H is only a subdominant DM candidate, with

$$\Omega_H h^2 < \Omega_c h^2 \quad (11)$$

(see [23, 31, 35]). In such a scenario, additional dark matter candidates would be needed in order to account for the missing relic density. In the results presented here, we apply XENON1T limits [58]². These supersede previous bounds applied e.g. in [31] in relevant regions of parameter space, and are therefore crucial for a correct determination of the available parameter space, especially for low dark masses.

Results from indirect detection experiments, e.g. Fermi-LAT [60], give less stringent constraints than collider and direct detection experiments discussed above [10, 35]. A number of planned DM indirect detection experiments, mainly the Cherenkov Telescope Array, will be able to probe the heavy mass region, with DM particle heavier than 500 GeV [61]. Furthermore, if the reported gamma-ray excess from the Galactic center is of DM origin [62], it can be explained by the IDM with dark matter masses near the Higgs resonance or around 72 GeV [63]. All dark matter variables were calculated with the use of `micrOmegas` version 4.3.5 [64].

3.2 Scan setup and limits

After fixing the value of M_h , and hence both λ_1 and m_{11}^2 , we are left with five independent input parameters for the scan: three masses of dark scalars M_{A,H,H^\pm} and two couplings, λ_{345}, λ_2 . In the initial setup of our scan, masses take values between 0 and 1 TeV, with M_H always being the lightest and $M_{H^\pm} \geq 70$ GeV. Unless stated otherwise, scalar couplings fall in the range of $\lambda_2 \in [0; 4.5], \lambda_{345} \in [-1.5; 4\pi]$.

In order to get interesting benchmark points we follow a procedure described in [23]. All constraints described in the previous section are checked in steps, with the aid of publicly available tools. In the process we track the impact of each exclusion criterion.

The first step contains a check through the 2HDMC in order to establish agreement with theoretical constraints (positivity, stability, perturbative unitarity). The same code is used to check the SM-like Higgs and electroweak gauge bosons widths, the decay rates of $h \rightarrow$ invisible, and $h \rightarrow \gamma\gamma$, properties of charged scalar (lifetime, mass) as well as the EWPT observables. Points that have passed the first step are then checked against limits from collider searches, in particular the Higgs signal strength limits, with the use of `HiggsBounds` and `HiggsSignals`. Points which passed the collider test are then confronted with limits from DM phenomenology, i.e. the relic density constraints with upper Planck bound (points that correspond to 100% of measured $\Omega_c h^2$ are selected at later stage) and direct detection limits from XENON1T, with the use of `micrOmegas`.

Although the IDM is one of the simplest extensions of the SM and has a limited number of parameters, it is still difficult to establish which constraint has the greatest impact on excluding the given point in parameter space. In the following, we point to some generic features that however can be used for a clear distinction in the model parameters space (see also [23]).

It is important to emphasize that the couplings that govern the production and decay processes at e^+e^- colliders are mainly determined by the electroweak parameters of the SM; the additional parameters in the potential do not play any significant role for the allowed scenarios. On the other side, the parameter λ_{345} is especially sensitive to constraints from dark matter observations. This nicely demonstrates the important complementarity of collider and astrophysical measurements in constraining the IDM parameter space.

We divide the discussion in two different subsections

²We use a digitized format of that data available from [59].

- (i) constraints on the masses of the dark scalars, with the constraint given in eqn. (11) for the dark matter relic density;
- (ii) additional limits we obtain when requiring exact relic density.

We only briefly discuss the second point here and refer to the literature (see e.g. [35]) for further details.

3.2.1 Limits on masses

The collider phenomenology of the IDM is mainly determined by the dark scalar masses, as all relevant production and decay channels are governed by electroweak couplings and the corresponding SM parameters. As dominant constraints for the regions for $M_H \leq M_h/2$ and $M_H \geq M_h/2$ originate from different sources, we will discuss these separately.

- In general, constraints arising from EWPT are of a great importance to our studies. As found in [23, 35, 65], mass splittings between inert particles are heavily limited by the S,T,U parameters. First, only moderate mass splittings are allowed by EWPT data, with preferred value of $M_{H^\pm} - M_A$ below 100 GeV. Also, there is a hierarchy between masses, with the charged scalar being the heaviest particle. The reverse relation is not excluded, however it will lead to a larger tension with combined S and T limits. In general, points with moderate mass splittings are preferred, especially for dark matter candidates with masses ≥ 300 GeV, where splittings between M_A and M_H are typically of order 10% or lower. For masses $M_H \leq 100$ GeV, we found that relatively large mass differences are allowed between the two neutral scalars. The mass hierarchy and constraints on mass splittings can influence cascade decays of inert particles.
- In addition to eqn.(8), the measurement of $h \rightarrow \gamma\gamma$ puts a lower limit on the charged Higgs mass as a function of λ_{345} , cf. e.g. [31].
- masses of DM particles below 45 GeV are excluded [23, 35]. For $M_H \leq M_h/2$ limits from the invisible branching ratio of the SM Higgs lead to relatively low values of λ_{345} , which in turn result in the relic density exceeding the measured value by orders of magnitude or the mass splittings changing electroweak gauge bosons widths³ significantly.
- for dark scalars with masses $\lesssim 100$ GeV, additional specific constraints are given by eqn.(9).

The parameters λ_2 and λ_{345} are also constrained from combined positivity, unitarity and global minimum conditions [66]. The exact value of λ_2 parameter would matter in studies that consider interaction between inert particles, for example for the astrophysical implications of self-interacting dark matter, or if the loop processes like $HH \rightarrow \gamma\gamma$ through the H^+H^- loop are considered, this is however beyond the scope of this work.

Dark matter constraints give major bounds on allowed values of λ_{345} . In general, $|\lambda_{345}| \lesssim 1.5$ for dark masses up to 1 TeV. For $M_H \lesssim M_h/2$, this limit decreases to $|\lambda_{345}| \lesssim 0.006$, due to the inclusion of results presented in [58]. Limits from Higgs signal strength measurements also limit

³See e.g. detailed discussions in [35].

this parameter, albeit less strongly than dark matter constraints. If we allow for a subdominant dark matter candidate, the parameter space largely opens up for regions where the dark matter relic density is much lower than the Planck value. Direct detection limits are then rescaled and therefore considerably relaxed (see also [23]). A prominent example for this is the region where $M_H \sim M_h/2$, leading to large annihilation cross sections. This broadens especially the allowed range for λ_{345} .

In summary, M_{H^\pm} and M_A are relatively degenerate throughout the allowed parameter space. The splittings between these and the dark matter candidate depend on the DM mass and can become quite large, especially for low M_H . The couplings λ_2 and λ_{345} do not play a significant role in collider phenomenology.

3.2.2 Requiring exact relic density

Requiring the model to render exact relic density, as specified by eqn.(10), puts additional constraints on the model. These are mainly on the coupling combination λ_{345} , but also affect the values of possible dark scalar masses in such a scenario.

- If H is the only source of DM in the Universe then it is possible to find good points only for masses $M_H \gtrsim 55 \text{ GeV}$;
- good points can then be obtained for $M_H \lesssim 75 \text{ GeV}$.
- For M_H larger than 500 GeV extreme fine-tuning of the dark masses is required in order to obtain exact relic density; cf. the discussion in [35]. The authors of that reference find that $\mathcal{O}(\text{GeV})$ mass splittings between the dark scalars would be required in order to obtain the correct relic density; in turn, this can lead to long-lived particles at the LHC. In our work, we do not study this particularly fine-tuned region in more detail.

4 Benchmark Points

As the aim of this note is to present benchmarks useful for further studies at linear colliders, we are particularly interested in points that provide an observable signal. For the possible signal we take the pair-production processes

$$e^+e^- \rightarrow H^+H^- \quad \text{and} \quad e^+e^- \rightarrow AH \quad (12)$$

for charged and neutral scalar production. The s-channel production $e^+e^- \rightarrow h \rightarrow AA$ is also possible, however it is suppressed by a small electron Yukawa coupling. The dark scalars H^\pm and A will then decay into a virtual or on-shell electroweak gauge boson and the dark matter candidate. Here, we first concentrate on center-of-mass energies of $\sqrt{s} \in \{250; 380; 500\} \text{ GeV}$, therefore constraining ourselves to scenarios where either $M_{H^\pm} \leq 250 \text{ GeV}$ or $M_H + M_A \leq 500 \text{ GeV}$ (or both). In section 5, we extend the analysis to contain higher dark scalar masses, in order to investigate the collider reach of the high energy ILC at 1 TeV and higher energy stages of CLIC at 1.5 TeV and 3 TeV [67]. In this work, we consider benchmarks with both on-shell and off-shell intermediate gauge bosons, as these differ in the collider phenomenology, and different cut strategies have to be applied.

Our benchmark selection was done in the following steps:

1. Benchmark candidates were generated by employing the scan presented in [23], with updated experimental constraints as discussed above. We selected about 7500 benchmark candidates which fulfill all constraints (we allow for under-abundant dark matter, therefore relaxing bounds from direct detection considerably in certain regions of parameter space).
2. We then calculated the production cross sections at 250, 380 and 500 GeV center-of-mass energies for processes (12); we required a minimal production cross section of 10 fb to classify a point as "accessible" for a certain process/energy stage;
3. if possible, we required a high-enough relic density, providing at least 50% of the value observed by the Planck collaboration;
4. finally we selected benchmark points corresponding to different accessibility at the subsequent energy stages and different kinematical configurations, namely on-shell vs off-shell intermediate gauge bosons.

The calculation of cross sections was performed using input files generated by **SARAH** 4.13.0 [68–70] and **SPheno** 4.0.3 [71, 72], which were passed to **WHizard** 2.2.8 [73, 74]. Initial state radiation was taken into account but not the beam luminosity spectra.

Point 2 above allows us to categorize different classes of benchmarks, which we label "XYZ" in the following, with X=1(2) corresponding to 1 (2) production processes accessible at 250 GeV, while Y and Z are defined accordingly for 380 GeV and 500 GeV. Within a certain category, we then considered different mass splitting configurations, in order to cover all possible typical parameter configurations leading to distinct collider signatures that can be generated by the IDM. The final selection of benchmark points, focusing on kinematic properties and selection criteria, is given in table 1. The table also contains the complete set of independent parameters for each point, as well as the relic density.

In our selection, BP1 is an example for a relatively small mass splitting, that forces the intermediate gauge boson to be off-shell. Other benchmark points, as e.g. BP9, allow for on-shell decays in both channels. However, these force the corresponding dark scalar masses to be $\mathcal{O}(150 \text{ GeV})$, therefore leading to smaller production cross sections.

Figure 1 shows the initial benchmark candidates, that obey all current constraints, in the $(M_{H^+} - M_H; M_A - M_H)$ plane. All points form a narrow band corresponding to $M_A \lesssim M_{H^\pm}$. Our chosen benchmark points, also indicated in Fig. 1 (red points) cover mass gaps up to about 250 GeV only, due to the required minimal cross section (see point 2 above). Notice that for most selected benchmark points the DM candidate is relatively light, with a mass below 80 GeV.

Tables 2 and 3 show the production cross sections at various center-of-mass energies for all benchmark scenarios. These indicate promising prospects of detection at future linear colliders. Because A is always a lighter particle, neutral channels are usually accessible at lower energies than charged ones. If both channels are accessible, the cross section for charged scalar pair-production is usually larger than for the neutral ones.

5 Extending to higher mass scales

So far, we have discussed IDM scenarios that are accessible at center-of-mass energies up to 500 GeV, with a mass range of $M \lesssim 250 \text{ GeV}$ for all dark scalars. However, the parameter space of the IDM

No.	M_H	M_A	M_{H^\pm}	Z on-shell	W on-shell	DM >50%	λ_2	λ_{345}	$\Omega_H h^2$
222									
BP1	72.77	107.803	114.639			✓	1.44513	-0.00440723	0.12007
BP2	65	71.525	112.85			✓	0.779115	0.0004	0.070807
BP3	67.07	73.222	96.73			✓	0	0.00738	0.061622
122									
BP4	73.68	100.112	145.728			✓	2.08602	-0.00440723	0.089249
BP6	72.14	109.548	154.761		✓	✓	0.0125664	-0.00234	0.11708
112									
BP7	76.55	134.563	174.367		✓		1.94779	0.0044	0.031402
BP8	70.91	148.664	175.89		✓	✓	0.439823	0.0051	0.124
BP9	56.78	166.22	178.24	✓	✓	✓	0.502655	0.00338	0.081268
BP23	62.69	162.397	190.822	✓	✓	✓	2.63894	0.0056	0.064038
022									
BP10	76.69	154.579	163.045		✓		3.92071	0.0096	0.028141
BP11	98.88	155.037	155.438				1.18124	-0.0628	0.0027369
BP12	58.31	171.148	172.96	✓	✓		0.540354	0.00762	0.0064099
012									
BP13	99.65	138.484	181.321		✓		2.46301	0.0532	0.001255
BP14	71.03	165.604	175.971	✓	✓	✓	0.339292	0.00596	0.11841
BP15	71.03	217.656	218.738	✓	✓	✓	0.766549	0.00214	0.12225
011									
BP16	71.33	203.796	229.092	✓	✓	✓	1.03044	-0.00122	0.12214
002									
BP18	147	194.647	197.403				0.387	-0.018	0.0017718
BP19	165.8	190.082	195.999				2.7675	-0.004	0.0028405
BP20	191.8	198.376	199.721				1.5075	0.008	0.008494
001									
BP21	57.475	288.031	299.536	✓	✓	✓	0.929911	0.00192	0.11946
BP22	71.42	247.224	258.382	✓	✓	✓	1.04301	-0.00406	0.12428

Table 1: In all benchmarks $M_h = 125.1$ GeV. Bold font denotes BP with 100% DM relic density. Accessibility categories are also shown (see text for details). Note that BP5 and BP17 were excluded by the updated XENON1T limits [58].

No.	M_H	M_A	M_{H^\pm}	$\sigma(250)$	$\sigma(380)$	$\sigma(500)$	$BR_{H^+H^- \rightarrow W^+H}$
BP1	72.77	107.803	114.639	23.7	97.8	82.6	> 0.99
BP2	65	71.525	112.85	30.4	101	83.9	0.66
BP3	67.07	73.222	96.73	108	127	95.3	0.75
BP4	73.68	100.112	145.728	-	46.7	59.9	0.92
BP6	72.14	109.548	154.761	-	33.3	53.2	0.99
BP7	76.55	134.563	174.367	-	9.59	38.9	> 0.99
BP8	70.91	148.664	175.89	-	8.16	37.8	> 0.99
BP9	56.78	166.22	178.24	-	6.13	36.1	> 0.99
BP10	76.69	154.579	163.045	-	22.3	47.1	> 0.99
BP11	98.88	155.037	155.438	-	32.4	52.7	1
BP12	58.31	171.148	172.96	-	11	39.9	1
BP13	99.65	138.484	181.321	-	3.79	33.9	0.99
BP14	71.03	165.604	175.971	-	8.09	37.7	> 0.99
BP15	71.03	217.656	218.738	-	-	10.5	1
BP16	71.33	203.796	229.092	-	-	5.64	> 0.99
BP18	147	194.647	197.403	-	-	23.1	1
BP19	165.8	190.082	195.999	-	-	24	> 0.99
BP20	191.8	198.376	199.721	-	-	21.6	1
BP23	62.69	162.397	190.822	-	-	27.4	> 0.99

Table 2: Production cross sections in fb for on-shell charged scalar pair-production, $e^+e^- \rightarrow H^+H^-$, for the center-of-mass energies considered in this work. We only list benchmark points with at least one non-zero production cross section. We also display the branching ratio $H^+ \rightarrow W^+H$ (the other possible channel, $H^+ \rightarrow W^+A$, is suppressed for most BPs). The displayed branching ratios were calculated using 2HDMC.

No.	M_H	M_A	M_{H^\pm}	$\sigma(250)$	$\sigma(380)$	$\sigma(500)$
BP1	72.77	107.803	114.639	77.2	65.9	45.7
BP2	65	71.525	112.85	155	85.1	53.4
BP3	67.07	73.222	96.73	149	83.5	52.8
BP4	73.68	100.112	145.728	89.2	69.1	46.9
BP6	72.14	109.548	154.761	75.1	65.4	45.4
BP7	76.55	134.563	174.367	31.2	52.3	40.1
BP8	70.91	148.664	175.89	20	47.5	38.1
BP9	56.78	166.22	178.24	14.1	43	36
BP10	76.69	154.579	163.045	9.44	43	36.2
BP11	98.88	155.037	155.438	-	35.6	33.2
BP12	58.31	171.148	172.96	9.01	40.4	34.8
BP13	99.65	138.484	181.321	5.17	42.5	36.2
BP14	71.03	165.604	175.971	5.13	39.6	34.7
BP15	71.03	217.656	218.738	-	18.2	24.2
BP16	71.33	203.796	229.092	-	23.3	26.9
BP18	147	194.647	197.403	-	6.14	18.7
BP19	165.8	190.082	195.999	-	3.02	16.6
BP20	191.8	198.376	199.721	-	-	11.3
BP21	57.475	288.031	299.536	-	2.66	12.6
BP22	71.42	247.224	258.382	-	8.94	18.6
BP23	62.69	162.397	190.822	13.2	43.3	36.2

Table 3: Production cross sections in fb for on-shell neutral scalar pair-production, $e^+ e^- \rightarrow HA$, for the center-of-mass energies considered in this work. We only list benchmark points with at least one non-zero production cross section. The branching ratio $\text{BR}(A \rightarrow HZ^{(*)}) \approx 100\%$.

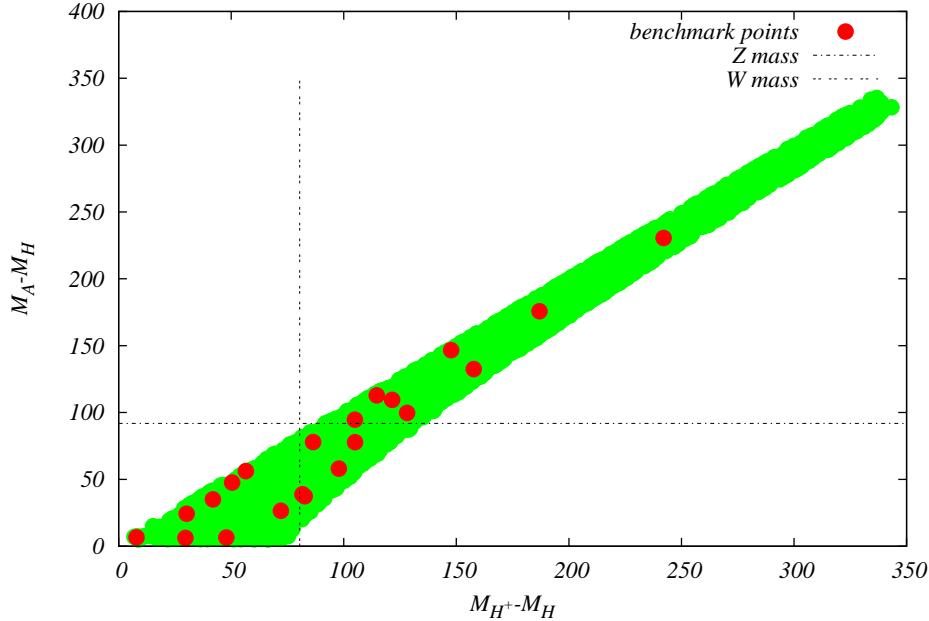


Figure 1: Distribution of benchmark candidate points (green) in the $(M_{H^+} - M_H; M_A - M_H)$ plane, after all constraints are taken into account, as well as selected benchmark points (red) in the same plane. The dashed lines indicate the electroweak gauge boson masses that distinguish between on- and off-shell decays of dark scalars. The relatively narrow band stems mainly from electroweak precision constraints.

largely opens up for higher dark scalar masses, especially as direct detection constraints are less strict and direct collider searches pose less stringent constraints.⁴ Therefore, in this section we consider high-mass benchmark points (HP) that can be explored at higher center-of-mass energies, e.g. at 1 TeV ILC or at the high-energy stages of the CLIC collider, at 1.5 TeV or 3 TeV.

As before, all benchmark points have passed theoretical and experimental constraints discussed in section 3. We now consider the nominal collider energies of 1 TeV, 1.5 TeV and 3 TeV. From about 6000 parameter points, we selected 20 benchmark points. The selection was done analogously to the low-energy case, aiming in addition to cover the whole mass range of the dark scalars up to 1 TeV. Benchmark points are summarized in table 4. The maximum mass splitting between the dark scalars is about 140 GeV, as the relic density decreases rapidly with the increasing mass difference (see sec. 3.2.2).

6 Conclusions

In this paper we have revisited and updated the available parameter space of the Inert Doublet Model. The model features an exact Z_2 symmetry which results in dark scalars that do not interact with SM fermions, and the lightest neutral scalar can serve as a promising dark matter particle. We

⁴Constraints stemming from the diphoton range exclude certain ranges in the M_{H^+}, λ_{345} plane, cf. e.g. [31], leading to a lower limit on the dark charged scalar mass.

No.	M_H	M_A	M_{H^\pm}	Z on-shell	W on-shell	DM >50%	λ_2	λ_{345}	$\Omega_H h^2$
HP1	176	291.36	311.96	✓	✓		1.4895	-0.1035	0.00072156
HP2	557	562.316	565.417			✓	4.0455	-0.1385	0.072092
HP3	560	616.32	633.48				3.3795	-0.0895	0.001129
HP4	571	676.534	682.54	✓	✓		1.98	-0.471	0.00056347
HP5	671	688.108	688.437				1.377	-0.1455	0.024471
HP6	713	716.444	723.045				2.88	0.2885	0.035152
HP7	807	813.369	818.001				3.6675	0.299	0.032393
HP8	933	939.968	943.787			✓	2.9745	-0.2435	0.09639
HP9	935	986.22	987.975				2.484	-0.5795	0.0027958
HP10	990	992.36	998.12			✓	3.3345	-0.051	0.12478
HP11	250.5	265.49	287.226				3.90814	-0.150071	0.00535
HP12	286.05	294.617	332.457				3.29239	0.112124	0.00277
HP13	336	353.264	360.568				2.48814	-0.106372	0.00937
HP14	326.55	331.938	381.773				0.0251327	-0.0626727	0.00356
HP15	357.6	399.998	402.568				2.06088	-0.237469	0.00346
HP16	387.75	406.118	413.464				0.816814	-0.208336	0.0116
HP17	430.95	433.226	440.624				3.00336	0.082991	0.0327
HP18	428.25	453.979	459.696				3.87044	-0.281168	0.00858
HP19	467.85	488.604	492.329				4.12177	-0.252036	0.0139
HP20	505.2	516.58	543.794				2.53841	-0.354	0.00887

Table 4: High-mass benchmark points (HPs) accessible at colliders with $\mathcal{O}(\text{TeV})$ center-of-mass energies. $M_h = 125.1 \text{ GeV}$ for all points. HP10 provides exact relic density.

No.	M_H [GeV]	M_A [GeV]	M_{H^\pm} [GeV]	$\sigma(e^+e^- \rightarrow H^+H^-)$			$\sigma(e^+e^- \rightarrow AH)$		
				1 TeV	1.5 TeV	3 TeV	1 TeV	1.5 TeV	3 TeV
HP1	176	291.36	311.96	13	9.9	3.4	8.6	5.1	1.6
HP2	557	562.316	565.417	-	3.1	2.6	-	1.4	1.1
HP3	560	616.32	633.48	-	1.6	2.4	-	1.1	1.1
HP4	571	676.534	682.54	-	0.68	2.2	-	0.77	1.1
HP5	671	688.108	688.437	-	0.59	2.2	-	0.32	0.98
HP6	713	716.444	723.045	-	0.16	2.1	-	0.11	0.93
HP7	807	813.369	818.001	-	-	1.8	-	-	0.79
HP8	933	939.968	943.787	-	-	1.4	-	-	0.6
HP9	935	986.22	987.975	-	-	1.2	-	-	0.57
HP10	990	992.36	998.12	-	-	1.2	-	-	0.52
HP11	250.5	265.49	287.226	15	11	3.5	7.8	4.9	1.6
HP12	286.05	294.617	332.457	11	9.4	3.3	6.5	4.6	1.5
HP13	336	353.264	360.568	8.5	8.6	3.3	4.3	3.9	1.4
HP14	326.55	331.938	381.773	6.7	8	3.2	4.9	4.1	1.5
HP15	357.6	399.998	402.568	5	7.5	3.1	3	3.5	1.4
HP16	387.75	406.118	413.464	4.2	7.2	3.1	2.4	3.3	1.4
HP17	430.95	433.226	440.624	2.4	6.4	3	1.3	2.9	1.3
HP18	428.25	453.979	459.696	1.3	5.9	3	1	2.8	1.3
HP19	467.85	488.604	492.329	0.09	5	2.8	0.21	2.4	1.3
HP20	505.2	516.58	543.794	-	3.7	2.7	-	2	1.2

Table 5: Production cross sections in fb for high-mass benchmark points at 1 TeV, 1.5 TeV and 3 TeV, for the production processes considered here.

took into account most recent experimental constraints from relic density and direct dark matter searches, including the latest XENON1T 2018 results, as well as collider bounds and theoretical constraints. Based on these updated results, we have provided benchmark scenarios accessible at the initial stages of future linear e^+e^- colliders (250 and 500 GeV ILC and 380 GeV CLIC) as well as benchmarks that can be tested at high-energy stages (1 TeV ILC and 1.5 and 3 TeV CLIC). In doing so we pursued the philosophy of covering the widest range of parameters and experimental signatures. We provide predictions of production cross sections at these energies, and supplement these with information about the branching fractions of the relevant decay modes. We encourage the LC groups to make use of these benchmark scenarios. Although the benchmarks have been defined with e^+e^- physics in mind, we strongly encourage our LHC experimental colleagues to consider these scenarios in the analysis of the current and upcoming LHC data.

Acknowledgements

The authors thank Jürgen Reuter and Wolfgang Kilian for useful comments regarding Whizard and the Sarah/Spheno interface. This research was supported in parts by the National Science Centre, Poland, the HARMONIA project under contract UMO-2015/18/M/ST2/00518 (2016-2019) and OPUS project under contract UMO-2017/25/B/ST2/00496 (2018-2020). The work of TR was partially supported by the National Science Foundation under Grant No. 1519045, by Michigan State University through computational resources provided by the Institute for Cyber-Enabled Research, and by grant K 125105 of the National Research, Development and Innovation Fund in Hungary. The work of WK was partially supported by the German Research Foundation (DFG) under grants number STO 876/4-1 and STO 876/2-2.

References

- [1] Carli Tancredi. ATLAS + ALICE highlights. Presented at ICHEP’2018, Seoul, Korea, Jul. 2018.
- [2] Rahatlou Shahram. CMS + LHCb highlights. Presented at ICHEP’2018, Seoul, Korea, Jul. 2018.
- [3] P. A. R. Ade et al. Planck 2015 results. XIII. Cosmological parameters. *Astron. Astrophys.*, 594:A13, 2016, 1502.01589.
- [4] Nilendra G. Deshpande and Ernest Ma. Pattern of Symmetry Breaking with Two Higgs Doublets. *Phys. Rev.*, D18:2574, 1978.
- [5] Qing-Hong Cao, Ernest Ma, and G. Rajasekaran. Observing the Dark Scalar Doublet and its Impact on the Standard-Model Higgs Boson at Colliders. *Phys. Rev.*, D76:095011, 2007, 0708.2939.
- [6] Riccardo Barbieri, Lawrence J. Hall, and Vyacheslav S. Rychkov. Improved naturalness with a heavy Higgs: An Alternative road to LHC physics. *Phys. Rev.*, D74:015007, 2006, hep-ph/0603188.

- [7] Laura Lopez Honorez, Emmanuel Nezri, Josep F. Oliver, and Michel H. G. Tytgat. The Inert Doublet Model: An Archetype for Dark Matter. *JCAP*, 0702:028, 2007, hep-ph/0612275.
- [8] Laura Lopez Honorez and Carlos E. Yaguna. The inert doublet model of dark matter revisited. *JHEP*, 09:046, 2010, 1003.3125.
- [9] Ethan M. Dolle and Shufang Su. The Inert Dark Matter. *Phys. Rev.*, D80:055012, 2009, 0906.1609.
- [10] A. Goudelis, B. Herrmann, and O. Stål. Dark matter in the Inert Doublet Model after the discovery of a Higgs-like boson at the LHC. *JHEP*, 09:106, 2013, 1303.3010.
- [11] Maria Krawczyk, Dorota Sokolowska, Pawel Swaczyna, and Bogumila Swiezewska. Constraining Inert Dark Matter by $R_{\gamma\gamma}$ and WMAP data. *JHEP*, 09:055, 2013, 1305.6266.
- [12] Erik Lundstrom, Michael Gustafsson, and Joakim Edsjo. The Inert Doublet Model and LEP II Limits. *Phys. Rev.*, D79:035013, 2009, 0810.3924.
- [13] Ethan Dolle, Xinyu Miao, Shufang Su, and Brooks Thomas. Dilepton Signals in the Inert Doublet Model. *Phys. Rev.*, D81:035003, 2010, 0909.3094.
- [14] Michael Gustafsson, Sara Rydbeck, Laura Lopez-Honorez, and Erik Lundstrom. Status of the Inert Doublet Model and the Role of multileptons at the LHC. *Phys. Rev.*, D86:075019, 2012, 1206.6316.
- [15] Mayumi Aoki, Shinya Kanemura, and Hiroshi Yokoya. Reconstruction of Inert Doublet Scalars at the International Linear Collider. *Phys. Lett.*, B725:302–309, 2013, 1303.6191.
- [16] Shu-Yu Ho and Jusak Tandean. Probing Scotogenic Effects in e^+e^- Colliders. *Phys. Rev.*, D89:114025, 2014, 1312.0931.
- [17] Abdesslam Arhrib, Yue-Lin Sming Tsai, Qiang Yuan, and Tzu-Chiang Yuan. An Updated Analysis of Inert Higgs Doublet Model in light of the Recent Results from LUX, PLANCK, AMS-02 and LHC. *JCAP*, 1406:030, 2014, 1310.0358.
- [18] Abdesslam Arhrib, Rachid Benbrik, and Naveen Gaur. $H \rightarrow \gamma\gamma$ in Inert Higgs Doublet Model. *Phys. Rev.*, D85:095021, 2012, 1201.2644.
- [19] Bogumila Swiezewska and Maria Krawczyk. Diphoton rate in the inert doublet model with a 125 GeV Higgs boson. *Phys. Rev.*, D88(3):035019, 2013, 1212.4100.
- [20] I. F. Ginzburg. Measuring mass and spin of Dark Matter particles with the aid energy spectra of single lepton and dijet at the e^+e^- Linear Collider. *J. Mod. Phys.*, 5:1036–1049, 2014, 1410.0869.
- [21] Genevieve Belanger, Beranger Dumont, Andreas Goudelis, Bjorn Herrmann, Sabine Kraml, and Dipan Sengupta. Dilepton constraints in the Inert Doublet Model from Run 1 of the LHC. *Phys. Rev.*, D91(11):115011, 2015, 1503.07367.

- [22] Nikita Blinov, Jonathan Kozaczuk, David E. Morrissey, and Alejandro de la Puente. Compressing the Inert Doublet Model. *Phys. Rev.*, D93(3):035020, 2016, 1510.08069.
- [23] Agnieszka Ilnicka, Maria Krawczyk, and Tania Robens. Inert Doublet Model in light of LHC Run I and astrophysical data. *Phys. Rev.*, D93(5):055026, 2016, 1508.01671.
- [24] Majid Hashemi, Maria Krawczyk, Saereh Najjari, and Aleksander F. Żarnecki. Production of Inert Scalars at the high energy e^+e^- colliders. *JHEP*, 02:187, 2016, 1512.01175.
- [25] P. Poulose, Shibananda Sahoo, and K. Sridhar. Exploring the Inert Doublet Model through the dijet plus missing transverse energy channel at the LHC. *Phys. Lett.*, B765:300–306, 2017, 1604.03045.
- [26] Amitava Datta, Nabanita Ganguly, Najimuddin Khan, and Subhendu Rakshit. Exploring collider signatures of the inert Higgs doublet model. *Phys. Rev.*, D95(1):015017, 2017, 1610.00648.
- [27] Majid Hashemi and Saereh Najjari. Observability of Inert Scalars at the LHC. *Eur. Phys. J.*, C77(9):592, 2017, 1611.07827.
- [28] Shinya Kanemura, Mariko Kikuchi, and Kodai Sakurai. Testing the dark matter scenario in the inert doublet model by future precision measurements of the Higgs boson couplings. *Phys. Rev.*, D94(11):115011, 2016, 1605.08520.
- [29] A. G. Akeroyd et al. Prospects for charged Higgs searches at the LHC. *Eur. Phys. J.*, C77(5):276, 2017, 1607.01320.
- [30] Neng Wan, Niu Li, Bo Zhang, Huan Yang, Min-Fu Zhao, Mao Song, Gang Li, and Jian-You Guo. Searches for Dark Matter via Mono-W Production in Inert Doublet Model at the LHC. *Commun. Theor. Phys.*, 69(5):617, 2018.
- [31] Agnieszka Ilnicka, Tania Robens, and Tim Stefaniak. Constraining Extended Scalar Sectors at the LHC and beyond. *Mod. Phys. Lett.*, A33(10n11):1830007, 2018, 1803.03594.
- [32] A. Belyaev, T. R. Fernandez Perez Tomei, P. G. Mercadante, C. S. Moon, S. Moretti, S. F. Novaes, L. Panizzi, F. Rojas, and M. Thomas. Advancing LHC Probes of Dark Matter from the Inert 2-Higgs Doublet Model with the Mono-jet Signal. 2018, 1809.00933.
- [33] Leonid Chuzhoy and Edward W. Kolb. Reopening the window on charged dark matter. *JCAP*, 0907:014, 2009, 0809.0436.
- [34] D. de Florian et al. Handbook of LHC Higgs Cross Sections: 4. Deciphering the Nature of the Higgs Sector. 2016, 1610.07922.
- [35] Alexander Belyaev, Giacomo Cacciapaglia, Igor P. Ivanov, Felipe Rojas-Abatte, and Marc Thomas. Anatomy of the Inert Two Higgs Doublet Model in the light of the LHC and non-LHC Dark Matter Searches. *Phys. Rev.*, D97(3):035011, 2018, 1612.00511.
- [36] Shuquan Nie and Marc Sher. Vacuum stability bounds in the two Higgs doublet model. *Phys. Lett.*, B449:89–92, 1999, hep-ph/9811234.

- [37] Bogumila Swiezewska. Inert scalars and vacuum metastability around the electroweak scale. *JHEP*, 07:118, 2015, 1503.07078.
- [38] Michael S. Chanowitz and Mary K. Gaillard. The TeV Physics of Strongly Interacting W's and Z's. *Nucl. Phys.*, B261:379–431, 1985.
- [39] I. F. Ginzburg and I. P. Ivanov. Tree-level unitarity constraints in the most general 2HDM. *Phys. Rev.*, D72:115010, 2005, hep-ph/0508020.
- [40] I. F. Ginzburg, K. A. Kanishev, M. Krawczyk, and D. Sokolowska. Evolution of Universe to the present inert phase. *Phys. Rev.*, D82:123533, 2010, 1009.4593.
- [41] Morad Aaboud et al. Measurement of the Higgs boson mass in the $H \rightarrow ZZ^* \rightarrow 4\ell$ and $H \rightarrow \gamma\gamma$ channels with $\sqrt{s} = 13$ TeV pp collisions using the ATLAS detector. *Phys. Lett.*, B784:345–366, 2018, 1806.00242.
- [42] Kuntal Mondal. Measurements of Higgs Boson Production and Properties in Di-photon Decay Channel Using Data Collected by CMS Detector at Center of Mass Energy of 13 TeV. *Springer Proc. Phys.*, 203:201–204, 2018.
- [43] Vardan Khachatryan et al. Search for Higgs boson off-shell production in proton-proton collisions at 7 and 8 TeV and derivation of constraints on its total decay width. *JHEP*, 09:051, 2016, 1605.02329.
- [44] Georges Aad et al. Measurements of the Higgs boson production and decay rates and constraints on its couplings from a combined ATLAS and CMS analysis of the LHC pp collision data at $\sqrt{s} = 7$ and 8 TeV. *JHEP*, 08:045, 2016, 1606.02266.
- [45] Philip Bechtle, Sven Heinemeyer, Oscar Stl, Tim Stefaniak, and Georg Weiglein. *HiggsSignals: Confronting arbitrary Higgs sectors with measurements at the Tevatron and the LHC*. *Eur. Phys. J.*, C74(2):2711, 2014, 1305.1933.
- [46] C. Patrignani et al. Review of Particle Physics. *Chin. Phys.*, C40(10):100001, 2016.
- [47] Guido Altarelli and Riccardo Barbieri. Vacuum polarization effects of new physics on electroweak processes. *Phys. Lett.*, B253:161–167, 1991.
- [48] Michael E. Peskin and Tatsu Takeuchi. A New constraint on a strongly interacting Higgs sector. *Phys. Rev. Lett.*, 65:964–967, 1990.
- [49] Michael E. Peskin and Tatsu Takeuchi. Estimation of oblique electroweak corrections. *Phys. Rev.*, D46:381–409, 1992.
- [50] I. Maksymyk, C. P. Burgess, and David London. Beyond S, T and U. *Phys. Rev.*, D50:529–535, 1994, hep-ph/9306267.
- [51] David Eriksson, Johan Rathsmann, and Oscar Stål. 2HDMC: Two-Higgs-Doublet Model Calculator Physics and Manual. *Comput. Phys. Commun.*, 181:189–205, 2010, 0902.0851.

- [52] M. Baak, J. Cúth, J. Haller, A. Hoecker, R. Kogler, K. Mönig, M. Schott, and J. Stelzer. The global electroweak fit at NNLO and prospects for the LHC and ILC. *Eur. Phys. J.*, C74:3046, 2014, 1407.3792.
- [53] Aaron Pierce and Jesse Thaler. Natural Dark Matter from an Unnatural Higgs Boson and New Colored Particles at the TeV Scale. *JHEP*, 08:026, 2007, hep-ph/0703056.
- [54] Philip Bechtle, Oliver Brein, Sven Heinemeyer, Georg Weiglein, and Karina E. Williams. HiggsBounds: Confronting Arbitrary Higgs Sectors with Exclusion Bounds from LEP and the Tevatron. *Comput. Phys. Commun.*, 181:138–167, 2010, 0811.4169.
- [55] Philip Bechtle, Oliver Brein, Sven Heinemeyer, Georg Weiglein, and Karina E. Williams. HiggsBounds 2.0.0: Confronting Neutral and Charged Higgs Sector Predictions with Exclusion Bounds from LEP and the Tevatron. *Comput. Phys. Commun.*, 182:2605–2631, 2011, 1102.1898.
- [56] Philip Bechtle, Oliver Brein, Sven Heinemeyer, Oscar Stål, Tim Stefaniak, Georg Weiglein, and Karina E. Williams. HiggsBounds – 4: Improved Tests of Extended Higgs Sectors against Exclusion Bounds from LEP, the Tevatron and the LHC. *Eur. Phys. J.*, C74(3):2693, 2014, 1311.0055.
- [57] Philip Bechtle, Sven Heinemeyer, Oscar Stål, Tim Stefaniak, and Georg Weiglein. Applying Exclusion Likelihoods from LHC Searches to Extended Higgs Sectors. *Eur. Phys. J.*, C75(9):421, 2015, 1507.06706.
- [58] E. Aprile et al. Dark Matter Search Results from a One Tonne×Year Exposure of XENON1T. *Phys. Rev. Lett.*, 121(11):111302, 2018, 1805.12562.
- [59] Alexander Belyaev, James Blandford, and Daniel Locke. Phenodata database. <https://hepmdb.soton.ac.uk/phenodata>, Jan. 2017.
- [60] A. Albert et al. Searching for Dark Matter Annihilation in Recently Discovered Milky Way Satellites with Fermi-LAT. *Astrophys. J.*, 834(2):110, 2017, 1611.03184.
- [61] Farinaldo S. Queiroz and Carlos E. Yaguna. The CTA aims at the Inert Doublet Model. *JCAP*, 1602(02):038, 2016, 1511.05967.
- [62] M. Ackermann et al. The Fermi Galactic Center GeV Excess and Implications for Dark Matter. *Astrophys. J.*, 840(1):43, 2017, 1704.03910.
- [63] Benedikt Eiteneuer, Andreas Goudelis, and Jan Heisig. The inert doublet model in the light of Fermi-LAT gamma-ray data: a global fit analysis. *Eur. Phys. J.*, C77(9):624, 2017, 1705.01458.
- [64] D. Barducci, G. Belanger, J. Bernon, F. Boudjema, J. Da Silva, S. Kraml, U. Laa, and A. Pukhov. Collider limits on new physics within micrOMEGAs_4.3. *Comput. Phys. Commun.*, 222:327–338, 2018, 1606.03834.
- [65] Laura Lopez Honorez and Carlos E. Yaguna. A new viable region of the inert doublet model. *JCAP*, 1101:002, 2011, 1011.1411.

- [66] Bogumila Swiezewska. Yukawa independent constraints for two-Higgs-doublet models with a 125 GeV Higgs boson. *Phys. Rev.*, D88(5):055027, 2013, 1209.5725. [Erratum: *Phys. Rev.*D88,no.11,119903(2013)].
- [67] M J Boland et al. Updated baseline for a staged Compact Linear Collider, 2016, 1608.07537.
- [68] Florian Staub. SARAH 3.2: Dirac Gauginos, UFO output, and more. *Comput. Phys. Commun.*, 184:1792–1809, 2013, 1207.0906.
- [69] Florian Staub. SARAH 4 : A tool for (not only SUSY) model builders. *Comput. Phys. Commun.*, 185:1773–1790, 2014, 1309.7223.
- [70] Florian Staub. Exploring new models in all detail with SARAH. *Adv. High Energy Phys.*, 2015:840780, 2015, arXiv:1503.04200.
- [71] Werner Porod. SPheno, a program for calculating supersymmetric spectra, SUSY particle decays and SUSY particle production at e+ e- colliders. *Comput. Phys. Commun.*, 153:275–315, 2003, hep-ph/0301101.
- [72] W. Porod and F. Staub. SPheno 3.1: Extensions including flavour, CP-phases and models beyond the MSSM. *Comput. Phys. Commun.*, 183:2458–2469, 2012, 1104.1573.
- [73] Mauro Moretti, Thorsten Ohl, and Jurgen Reuter. O’Mega: An Optimizing matrix element generator. pages 1981–2009, 2001, hep-ph/0102195.
- [74] Wolfgang Kilian, Thorsten Ohl, and Jurgen Reuter. WHIZARD: Simulating Multi-Particle Processes at LHC and ILC. *Eur. Phys. J.*, C71:1742, 2011, 0708.4233.